Sand bed roughness in the nearshore

Edith L. Gallagher
Franklin and Marshall College, Lancaster, Pennsylvania, USA

E. B. Thornton and T. P. Stanton
Naval Postgraduate School, Monterey, California, USA

Received 5 August 2001; revised 11 June 2002; accepted 3 September 2002; published 21 February 2003.

[1] Measurements made using sonar altimeters mounted on an amphibious surveying vehicle are analyzed for root-mean-square (RMS) bedform roughness. Observations for 22 days over a 500 m × 700 m area are used to quantify the cross-shore distribution of roughness and its variability. Large bedforms (with amplitudes 5–50 cm) occur frequently in shallow water (<2 m water depth). However, the patchiness of these bedforms is also largest in shallow water. This is likely owing to the spatial and temporal variability of the waves and currents, of the sediment grain size distributions, and of the large-scale nearshore morphology. Large bedforms were observed to exist only for mobility numbers <150, above this threshold the RMS roughness was <2 cm and the bed was interpreted to have transitioned to sheet flow conditions. However, the state of the bed (e.g., large ripples, small ripples, flat bed) was not predictable for mobility numbers between about 30 and 150. Existing models for orbital ripples do not predict the observed large bedforms and have little predictive skill for these data. *INDEX TERMS:* 4546 Oceanography: Physical: Nearshore processes; 4558 Oceanography: Physical: Sediment transport; 3020 Marine Geology and Geophysics: Littoral processes; *KEYWORDS:* seafloor roughness, bedforms, nearshore, surf zone, megaripples, bed friction

Citation: Gallagher, E. L., E. B. Thornton, and T. P. Stanton, Sand bed roughness in the nearshore, *J. Geophys. Res.*, *108*(C2), 3039, doi:10.1029/2001JC001081, 2003.

1. Introduction

[2] Bedforms on a barred beach are highly variable, both spatially and temporally, but this variability is poorly understood. A better understanding of bedforms in the nearshore would be valuable for interpretation of sedimentary sequences in the geologic record and for estimating seafloor roughness and resulting friction factors when predicting wave energy dissipation, nearshore current generation, sediment transport, and the resulting bathymetry change.

[3] Bedforms generated by steady currents (e.g., in rivers) have been studied in detail and regime diagrams can be used to determine roughly what types of bedforms will appear under certain flow conditions [e.g., *Middleton and Southard*, 1984; *Fredsoe and Deigaard*, 1992]. Bedform regimes under purely oscillatory flow also have been identified [e.g., *Clifton*, 1976; *Nielsen*, 1992]. However, in the natural surf zone, steady currents, wave driven oscillatory currents, wave asymmetries, and breaking-induced turbulence combine to create a complicated environment for sediment transport and bedform development, and prediction of bed state is difficult. Owing to the difficulty in studying this high-energy and highly variable environment, few observations of seafloor morphology have been made and little is known about bedforms in the nearshore.

0148-0227/03/2001JC001081$09.00

[4] *Clifton et al.* [1971] made observations using SCUBA of the cross-shore variability of nearshore bedforms on an Oregon beach during relatively mild conditions. They observed that bedforms change in size, shape, and symmetry across the nearshore. Far offshore, where waves were sinusoidal and the water was deep (>5 m), small symmetric oscillatory ripples were observed (2–5 cm high, wavelengths of 10–20 cm, straight but short-crested). Progressing toward the shore, waves begin to shoal and the observed ripples became asymmetric. Just before breaking, where wave skewness (peaked wave crests with strong onshore-directed velocities and broad flat troughs with smaller offshore-directed velocities [*Elgar et al.*, 1988]) is maximum, megaripples were observed (30–100 cm high, wavelengths of 1–5 m, lunate shaped). Beneath the breaking waves, the bed was planar owing to large velocities, turbulence and sheet flow conditions. Inside the surf zone, oscillatory velocity asymmetries, turbulence and steady currents create a complex fluid environment. Here, *Clifton et al.* [1971] observed a complex rough bed with large symmetric ripples (15–20 cm high, wavelengths of 30–60 cm, straight and long-crested), megaripples, and large holes (10–50 cm deep, 1–2 m across). Similar observations of cross-shore changes in bed state come from studies of strata within the bed [*Greenwood and Sherman*, 1986; *Davidson-Arnott and Greenwood*, 1976].

[5] More recently, *Hay and Wilson* [1994] observed changing bedform regimes in the nearshore with a rotating

side-scan sonar at a fixed location. As the wave energy decreased at the end of a storm, their instrument frame went from being inside the surf zone, with large waves breaking far offshore, to being outside the surf zone as the waves became smaller and broke closer to shore. They observed flat beds, small regular vortex ripples, cross ripples (both large and small ripples) and megaripples. Timescales for changes in bedform regimes were on the order of 1–3 hours. *Thornton et al.* [1998] made observations with a side-scan sonar and a single altimeter mounted on an amphibious surveying vehicle (the CRAB, see Figure 1). They observed highly variable bedforms in both the cross-shore and alongshore. Some of the observed patterns were similar to those of *Clifton et al.* [1971], but some were quite different.

[6] *Clifton* [1976] developed a regime model for bedforms under waves in the nearshore, which depends on peak flow velocity under waves u_m, flow asymmetry Δu_m (defined as the difference between the maximum forward flowing velocity and the maximum backward flowing velocity under a wave), wave period and sediment size. However, he acknowledged that his model did not include combined flow (waves plus currents), was poorly tested for breaking waves and high-energy conditions, and was approximate and should be used cautiously as a predictive tool. This model was developed for use in interpreting sedimentary structures and therefore ancient flow conditions. This type of model also would be useful in predicting bed configuration under shoaling and breaking waves. Models which predict the energy transformation of waves as they enter shallow water and the wave-induced circulation in the nearshore often include roughness owing to sand grains, some include roughness owing to sediment motion in the boundary layer, few include morphology-induced roughness [*Nicholson et al.*, 1997; *Young and Gorman*, 1995], and none consider the large features such as megaripples. This is owing to the lack of any theory to quantitatively predict the roughness for any given conditions.

[7] In this paper, unique observations of large bedforms are used to characterize the roughness of the seafloor in the nearshore. The observations of *Clifton et al.* [1971] are shown to be one case of cross-shore variation in bed morphology. Similarities between these observations and previous observations suggest that bedform processes are similar in natural surf zones. This more comprehensive data set is used to show that temporal variability and spatial patchiness are large. An average observed cross-shore roughness profile and its variability are discussed. The working hypothesis for this study, as well as all the previous work discussed above, is that the state of the bed morphology is dependant in some predictable way on geological and hydrodynamical conditions. Thus, a cross-shore array of electromagnetic current meters is used to examine the dependence of roughness on the flow field. Interestingly, this intuitive hypothesis is only weakly supported by this study.

2. Observations

[8] The temporal and spatial variability of bedforms on a barred beach were studied for 5 weeks in September and October 1997 near Duck, N. C., during the SandyDuck nearshore field experiment. Approximately daily surveys of a 500 m × 700 m area were made with a linear, lagged array of seven sonar altimeters mounted along the rear cross beam of the CRAB, (Coastal Research Amphibious Buggy, Figure 1). The CRAB, with a footprint of about 8 m, is designed to measure the large-scale morphology (e.g., sandbars) using DGPS with an accuracy of 4 cm RMS in the vertical and 3 cm RMS in the horizontal. The survey area is measured along 20 cross-shore lines, which are separated by 20–50 m.

Figure 1. CRAB. The CRAB is about 12 m tall, 8 m wide at the rear wheels (forward is toward the left), and the diameter of the tires is about 1.7 m. It is shown during the SandyDuck nearshore field experiment with an array of downward looking sonar altimeters mounted (on pipes) across the rear cross beam. The separations between the altimeters in the lagged array (from left to right) are 1.8, 1.5, 0.6, 0.15, 0.3, and 0.9 m. See http://www.frf.usace.army.mil for more information on the CRAB.

[9] The altimeters (1 MHz with automatic gain control [*Gallagher et al.*, 1996]) have <1 mm vertical resolution, but an effective resolution of ~2 cm (peak to peak). This is owing to the variability of the sediment bed, for example, dilation, bedload transport, and grain roughness [*Gallagher et al.*, 1996]. The altimeters are sampled at 48 Hz and, with CRAB speeds of 0.5–1 m/sec, the bed is sampled every 1–2 cm. The data are corrected for the motion of the CRAB

using pitch, roll, and yaw measurements (*Thornton et al.* [1998] found that these corrections were small O(1cm)) and, because there are spurious acoustic returns from the water column, a median filter is applied [*Thornton et al.*, 1998].

[10] The altimeter data and CRAB profiles are time synced and combined to give detailed cross-shore profiles, which include both large-scale (bars) and smaller-scale (megaripples) morphology (e.g., Figure 2a), with an effective vertical and cross-shore resolution of 2–4 cm. The separation of sonar altimeters in the lagged array ranges from 0.15–5 m (Figure 1) making resolution of megaripple length scales possible. However, length scales will not be discussed here. In this paper, vertical relief (RMS roughness) averaged over the seven sonar altimeters will be examined, thus alongshore resolution of roughness is determined by separation between the CRAB survey lines (20–50 m). In addition, a cross-shore array of electromagnetic current meters was used to examine the flow field.

[11] Observations of bedforms using the sonar altimeters sometimes agree with *Clifton et al.*'s [1971] observations of bedforms in the nearshore (suggesting similarities in the bed processes between the two different beaches). For example, in Figure 2a, a cross-shore profile from one sonar altimeter has a relatively smooth bed furthest offshore (x > 260 m, small ripples are poorly resolved so the distinction between small ripples and flat bed is not made), and has large bedforms just before the bar (x = 220–260 m). On the outer slope of the bar, where waves shoal and possibly break (x = 175–220 m), the bed is quite smooth, likely owing to high velocities near the bed and resulting sheet flow conditions. Inside the surf zone (x = 130–175 m) large bedforms are observed again.

[12] The large bedforms observed in Figure 2a are megaripples [*Clifton et al.*, 1971] and, as shown in detail in Figure 2b, have cross-shore lengths of about 2 m and amplitudes of 20–40 cm. The flat bed further offshore is shown in detail in Figure 2c. In general, spectra of short (∼10 m) cross-shore sections of the seafloor in the nearshore have a peak at low wave number (wavelengths of 1–5 m) and decay with increasing wave number (Figures 2d and 2e, from the 10-m long, high-pass filtered profiles in Figures 2b and 2c, dashed lines, and averaged for the seven sonars). During SandyDuck, wave-orbital ripples (heights of 1–10 cm, lengths of 0.1–1 m) were often visible but not always well resolved with the CRAB altimeters, so discussion of the wave-orbital ripple band will not be made in detail. Note that the orbital ripple band is included in the bed roughness estimation (below), but because the features are relatively small, their contribution to the total variance of the seafloor (the integrated spectrum) is small. Thus, bed fluctuations in the megaripple band are the most energetic, and megaripples are the largest source of bed variability at scales <10 m.

[13] The RMS bed level fluctuation is calculated as the square root of the integrated spectrum averaged over the seven altimeters (Figures 2d and 2e), giving an estimate of variability over the 10 m-long sections of bed in Figures 2b and 2c. Using overlapping, 10 m-long sections of bed profile, the RMS bed roughness is calculated every 1 m. The amplitude variation of bedforms across the profile in Figure 2a is well characterized by the RMS bed roughness profile (Figure 2f), where the large bedforms (x = 220–270 m and x = 130–175 m) have an RMS roughness of 7–10 cm and the smooth portions of the bed (and possibly small ripples) have an RMS roughness of <2 cm. The visually observed bedform amplitudes (Figure 2b and *Clifton et al.* [1971]) and the measured RMS roughness values differ by about a factor of 4 because the ripple height distribution is approximately Rayleigh [*Thornton et al.*, 1998].

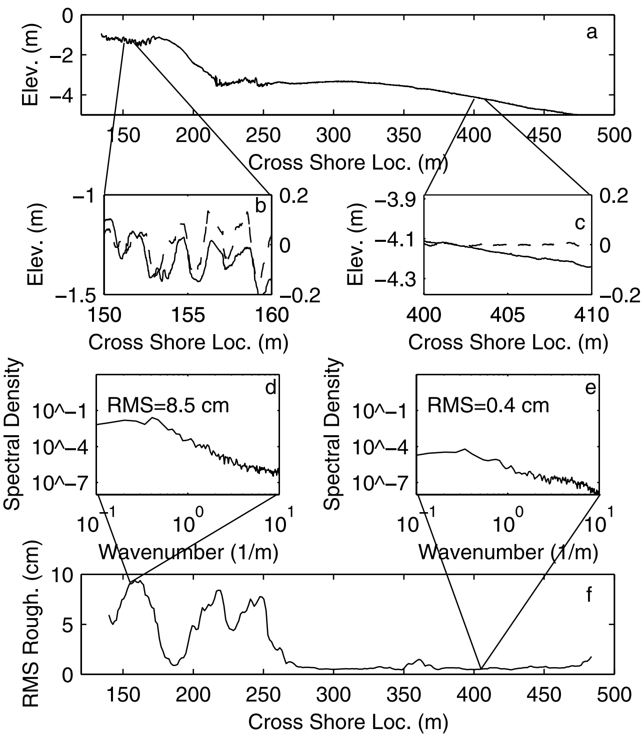

Figure 2. (a) Example of a combined (CRAB plus altimeter) cross-shore profile (October 7, y = 1030 m in Figure 3, H_S = 0.44 m) with elevation below mean sea level versus cross-shore location (see http://www.frf.usace.army.mil for more information on the Field Research Facility and the coordinate frame). (b–c) Solid lines are examples of 10-m long sections of Figure 2a (cross-shore locations x = 150–160 m and x = 400–410 m). These data are high-pass filtered (dashed lines) with a cutoff wavelength of 10 m. (d–e) Bed elevation spectra of the high passed sections (dashed lines in Figures 2b and 2c) averaged over seven sonars. Because the seven profiles are not independent measures of bed forms (correlations between sensors in the array are >0.6 for length-scales <1 m), the effective DOF ∼ 10. The square root of the variance from integrated spectra gives the RMS roughness. (f) RMS roughness versus cross-shore distance. The RMS is calculated every 1 m from overlapping (90%) 10-m long sections (as in panel 2b), to produce this RMS roughness profile from the depth profile in panel 2a.

[14] The daily survey area consists of 20 grid lines that extend from the shoreline to about 5 m water depth. Thus, for each daily CRAB survey, 20 roughness profiles are calculated and a map of RMS roughness is generated (Figure 3, using linear interpolation and MATLAB plotting routines). Also shown in Figure 3 are depth contours, which outline the large-scale bathymetry (black lines). During the SandyDuck experiment there were two bars, one in 3.5 m water depth at

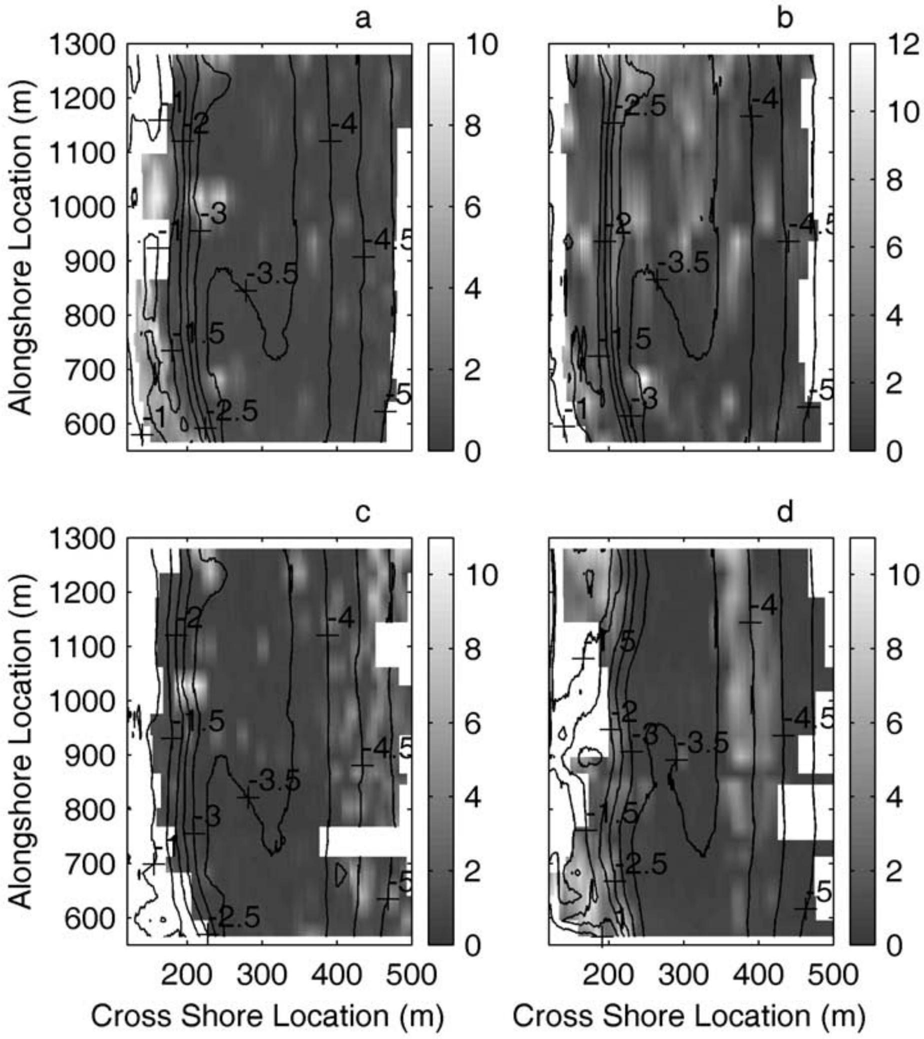

Figure 3. Maps of RMS roughness (centimeters) for the 500 m × 700 m survey area. Black lines show contours of large-scale bathymetry. Daily surveys of the area with the CRAB (Figure 1) consisted of 20 grid lines, thus 20 roughness profiles (e.g., Figure 2f is from y = 1030 m in Figure 3a) are used to generate these maps. (a) October 7, H_S = 0.44 m. (b) October 2, H_S = 0.88 m. (c) October 16, H_S = 1.65 m. (d) October 25, H_S = 0.75 m.

about x = 300 m and another in 1 m water depth at about x = 180 m. The outer bar was broad and flat, whereas the inner bar was better defined with a steep offshore slope (1/15). This large-scale morphology did not change significantly for the duration of the observations presented here.

2.1. Spatial Patterns

[15] The profile in Figure 2f is from alongshore location y = 1030 m in Figure 3a, and the described pattern from *Clifton et al.* [1971] is not consistent throughout the survey area. The bedforms in the outer trough (x = 220–260 m) are only seen at that location (and a couple others, y = 680, 1280 m) as a small patch of bedforms. The observed roughness distribution in Figure 3a is typical, with roughness highest in shallow water and patches in deeper water. However, there are variations on this pattern. An example when the offshore roughness patches were more prevalent is shown in Figure 3b. Large roughness on the offshore face of the outer bar and almost no roughness in shallow water are shown in Figure 3c. A fourth example shows large bedforms on both the outer face of the outer bar and in the inner trough (Figure 3d).

[16] The significant wave height H_S, measured in 8 m water depth, is shown in Figure 4 and the survey times of these four examples are represented by the dotted lines. These observations suggest that large bedforms are prevalent in the nearshore, but their spatial distribution changes. It is hypothesized that the reasons for variations in roughness distribution include changes in the offshore wave height (and resulting changes in cross-shore distribution of wave and current magnitudes), patchiness of sediments, and 3-D variations in the flow field, large-scale morphology, and wave breaking. The observations of *Clifton et al.* [1971], *Clifton* [1976], *Hay and Wilson* [1994] and *Thornton et al.* [1998] are in agreement with this hypothesis and provide specific cases from different surf zones with bed configuration depending, at least qualitatively, on the variables mentioned above.

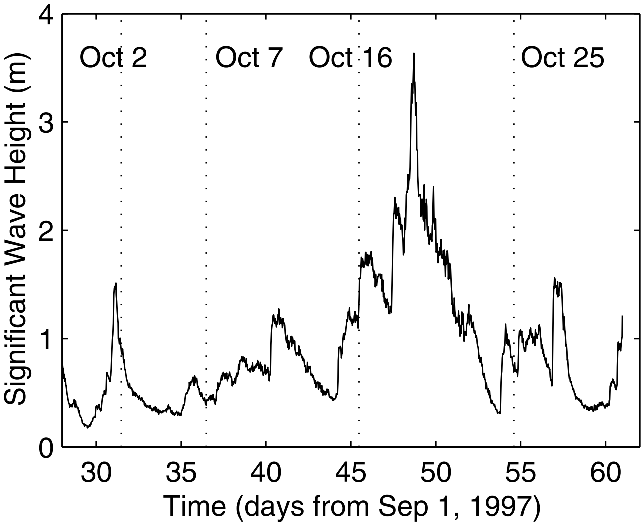

Figure 4. Significant wave height measured in 8 m water depth for the SandyDuck experiment. Vertical dotted lines show the times for the surveys shown in Figures 3 and 5.

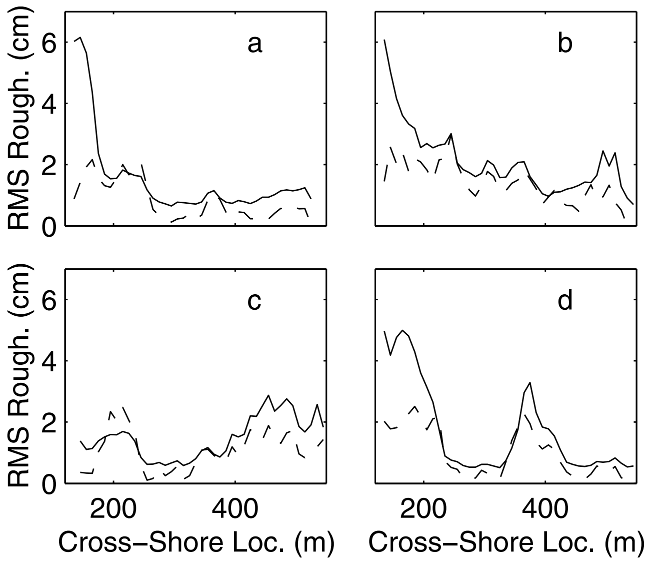

Figure 5. Alongshore-averaged RMS roughness versus cross-shore distance. Averaging the RMS roughness maps (e.g., Figure 3) in the alongshore direction gives a single daily mean RMS roughness profile (solid line) and its standard deviation (dashed line). (a) October 7, H_S = 0.44 m. (b) October 2, H_S = 0.88 m. (c) October 16, H_S = 1.65 m. (d) October 25, H_S = 0.75 m.

[17] To examine the cross-shore variation of roughness, each daily roughness map (e.g., Figure 3) was averaged in the alongshore to give a mean daily roughness profile. Four mean profiles (corresponding to maps in Figure 3) and their standard deviations are shown in Figure 5. In Figure 5a, the alongshore-averaged seafloor roughness is observed to be highest in the shallow water ($x < 200$ m) inside the inner bar, and the relatively low standard deviation indicates that this is consistent throughout the survey area (as can be seen in Figure 3a). However, for x = 200–250 m, the standard deviation is similar in magnitude to the mean roughness, (i.e., the variation is the same size as the roughness) indicating the lower roughness values are not consistent throughout the survey area. This relatively high standard deviation is owing to the patches in Figure 3a (x = 200–260 m, y = 1030 m, y = 1285 m, and y = 680 m). The significant wave height measured in 8 m water depth for this day was H_S = 0.44 m (October 7, Figure 4).

[18] Figures 5b–5d show alongshore-mean roughness and standard deviation profiles corresponding to the examples in Figures 3b–3d. The same trend is seen in Figure 5b as in Figure 5a, but the roughness values and their standard deviations are larger across the profile. The large bedform patches irregularly distributed throughout the survey area during this small storm-wave event (October 2, H_S = 0.88 m, Figure 4) increased both the mean roughness and the spatial variability. The roughness in Figure 5c is dominant offshore (x = 400–500 m) and the shallow water bedforms are only patchy, as indicated by the relatively large standard deviation between x = 180–250 m (October 16, H_S = 1.65 m, Figure 4). High roughness levels from bedforms in both shallow water (x = 140–220 m) and much deeper water (x = 350–450 m) separated by a relatively smooth stretch of seafloor are seen in Figure 5d (October 25, H_S = 0.75 m, Figure 4). The standard deviation is similar to the mean profile indicating that, where bedforms exist, they are spatially variable.

[19] To further generalize the roughness in the nearshore, a single time-averaged (over the 22 daily alongshore-averaged roughness profiles, four of which are shown in Figure 5) profile is calculated to try to identify a suitable estimate of the cross-shore distribution of roughness in the nearshore (Figure 6). During this time the large-scale morphology did not change significantly, although the significant wave

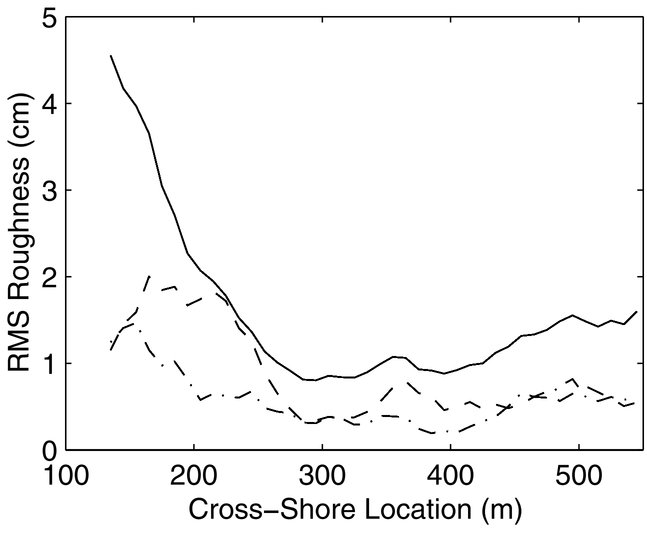

Figure 6. Time-average (over all days) of alongshore-averaged (each day) RMS bed roughness versus cross-shore distance. Averaging the daily mean RMS roughness profiles (e.g., Figure 5, solid lines) for 22 days gives a temporal average of the mean cross-shore RMS roughness (solid line). The dash-dotted line is standard deviation of this temporal average and represents the temporal variability. The dashed line is the mean of daily standard deviations (as represented by dashed lines in Figure 5) and represents the mean alongshore variability.

height ranged from 0.4–3.3 m (Figure 4). The time-averaged, alongshore-averaged roughness profile shows a significant increase in roughness associated with the shallow sandbar (x < 200 m, water depths < 2 m). This is likely due to bedforms generated by surf zone processes (wave asymmetries, combined currents and waves, breaking induced turbulence, etc.) The temporal variability, calculated as the standard deviation of the temporal average, is also largest in shallow water (dash-dotted line, Figure 6), as is the spatial variability calculated as the mean of alongshore standard deviations (e.g., dashed lines in Figures 5a–5d, shown as dashed line in Figure 6). The relatively high variability of bedforms in shallow water is likely owing to the high variability of surf zone processes in both space and time. Thus, the largest bedforms exist inside the surf zone, but their spatial distribution is patchier and their temporal variability is larger than the smaller offshore bedforms.

2.2. Fluid Forcing

[20] Consistent with *Clifton*'s [1976] regime-type model, as well as previous studies of bedforms in fluvial and purely oscillatory flows, these examples qualitatively support the hypothesis that the distribution of bedforms depends on the variation of the near bed fluid velocity as a function of wave shoaling and breaking. For example, comparing the bedforms in Figure 3d (H_S = 0.75) to those in Figure 3a (H_S = 0.44 m), the formation of a patch of bedforms between x = 350–420 m is hypothesized to be owing to increased near-bed water velocities at that depth associated with the higher waves. For even larger waves (Figure 3c, H_S = 1.65 m), the near-bed velocities and breaking induced turbulence in shallow water (depths < 2 m) become so large that the bed is planed off owing to sheet flow conditions and that the conditions for large bedform formation have moved to deeper water (depths > 4 m).

[21] To test this hypothesis, near bottom currents measured along an array at y = 830 m were used to calculate various fluid parameters. Roughness in the vicinity of the current meters (usually within about 15 m) was compared with mean velocity, RMS velocity, velocity skewness and asymmetry, as well as estimates of sediment transport [e.g., *Bailard*, 1981]. None of these quantities showed a significant relationship with the amplitude of the bedforms (not shown). Mobility number represents the ratio between the mobilizing force of the fluid and the stabilizing force of gravity and is given by

$$\Psi = \frac{\langle U^2 + V^2 \rangle}{(s-1)gD},$$

where U and V are the total (wave and current) instantaneous measured velocity components in the cross-shore and alongshore direction, s is the specific gravity (ratio of sediment density to water density, 2.65 for quartz sand), D is the mean grain diameter (surface samples taken twice during the experiment at the current meters), g is the acceleration of gravity, and $\langle\ \rangle$ denotes time average (over 3 hours for this study). Bed roughness is plotted versus Ψ in Figure 7a. For Ψ greater than about 150, the RMS roughness is less than 1 cm and megaripples do not exist. For $30 < \Psi < 150$, RMS roughness ranges from <1 cm to about 8 cm, indicating that both large bedforms and relatively smooth beds can occur.

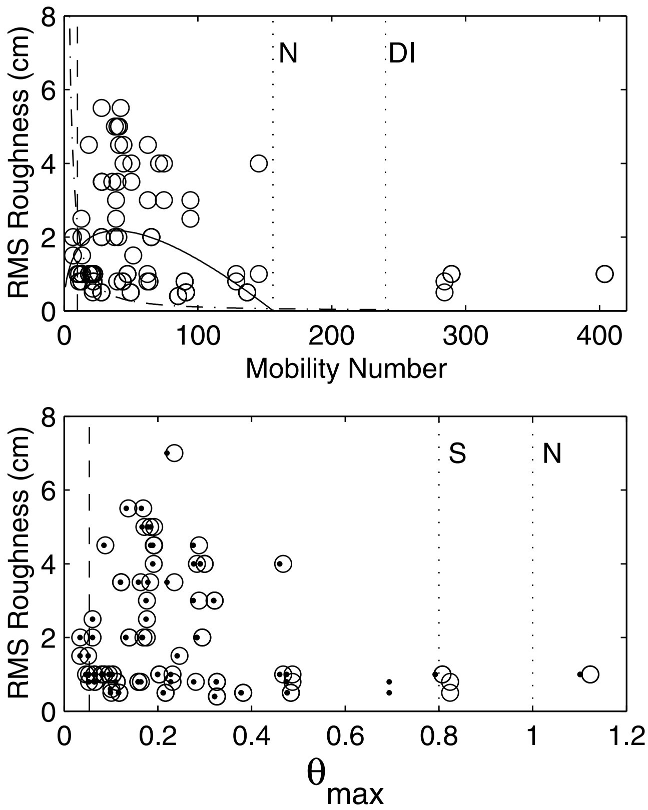

Figure 7. (a) RMS roughness versus mobility number. The solid line (regular waves) and the dash-dotted line (irregular waves) show the empirical relationships from *Nielsen* [1981] for wave-orbital ripple height. The dashed line shows the threshold for sediment motion for D = 0.2 mm. The dotted lines show the threshold for transition to sheet flow as reported by *Dingler and Inman* [1976] (DI), and *Nielsen* [1992] (N). (b) RMS roughness versus maximum combined flow Shields' parameter calculated following *Soulsby et al.*'s [1993] technique and using the models of (dots) *Fredsoe* [1984] and (open circles) *Grant and Madsen* [1979]. The dashed line shows the threshold of motion for D = 0.2 mm. The dotted lines show the threshold for transition to sheet flow as reported by *Soulsby* [1997] (S), and *Nielsen* [1992] (N).

When Ψ is less than about 30 the bed again becomes relatively smooth. The threshold of sediment motion (for D = 0.2 mm, typical at Duck) is about Ψ = 10 (dashed line, Figure 7a).

[22] Shields' parameter, a normalized estimate of shear stress, was also calculated. Maximum combined flow (i.e., wave and current) shear stress, τ, was calculated following the technique of *Soulsby et al.* [1993] and using the formulations of *Fredsoe* [1984] and *Grant and Madsen* [1979]. The input parameters for this calculation, which were derived from the data, include mean current velocity, wave-orbital velocity (RMS velocity was used), angle between the waves and currents, depth (h), and peak period. The drag coefficient for steady flow over a flat bed is estimated as

$$C_d = \left[\frac{0.4}{\ln(33h/k_s) - 1}\right]^2,$$

where the roughness length $k_s = 2.5D$, (for these conditions $C_d = 0.0008-0.0013$). This estimate of shear stress was then normalized to give Shields' parameter

$$\theta = \frac{\tau}{\rho(s-1)gD},$$

where ρ is the water density. The Shields' parameter is plotted versus roughness in Figure 7b.

[23] Mobility number and Shields parameter are commonly used as nondimensional measures of sediment transport conditions and bed state. For example, *Nielsen* [1981] suggested that orbital ripple height (in quartz sediments) is dependent on mobility number, based on field and laboratory observations. He proposed an empirical dependence for regular waves

$$\frac{\eta}{A} = 0.275 - 0.022\Psi^{0.5} \quad \text{for } \Psi < 156$$

(with $\eta = 0$ for $\Psi > 156$), and for irregular waves

$$\frac{\eta}{A} = 21\Psi^{-1.85},$$

where η is the ripple height and A is the orbital amplitude of the fluid near the bed. These estimates of bedform height are divided by $\sqrt{2}$ so they are comparable with observed RMS bed roughness and are plotted in Figure 7a. Typical conditions at Duck are used (0.2 mm sand and 10 s wave period) and the results were not sensitive to reasonable changes in these values.

3. Discussion

[24] Existing models for ripples under purely wave driven conditions do not predict the occurrence of large bedforms [*Li and Amos*, 1999]. For example, the empirical expression for wave-orbital ripple height under regular waves [*Nielsen*, 1981] indicates the existence of wave-orbital ripples for the same range of mobility numbers where megaripples, large wave ripples, and possibly wave-orbital ripples are observed, but does not suggest the variability of bed state that is observed (Figure 7). *Nielsen*'s [1981] relationship for irregular waves does not represent the observed bedforms.

[25] In steady flows, bedform regimes that change with flow, grain size, and water depth are well established, and flume experiments suggest there is a sharp transition from small ripples (vortex ripples) to larger ripples (megaripples and dunes) and then to sheet flow [e.g., *Middleton and Southard*, 1984; *Raudkivi*, 1990; *Reineck and Singh*, 1975]. In nature, small ripples are often superimposed on larger-scale ripples [e.g., *Southard et al.*, 1990; *Hay and Wilson*, 1994; *Li and Amos*, 1999]. Even in cases where they exist simultaneously, there is a definite break in size between small and large ripples [*Allen*, 1968; *Middleton and Southard*, 1984]. The observations presented here (Figure 7), under combined flows, do not show a sharp transition in ripple heights from small ripples to large ripples; that is, for $30 < \Psi < 150$ two distinct populations of ripple size are not observed.

[26] For $\Psi > 150$, large bedforms do not exist and this is interpreted as the transition to flat bed or sheet flow conditions. This is in general agreement with the literature. *Dingler and Inman* [1976] found the transition to sheet flow at $\Psi = 240$ (calculated using wave-orbital velocity amplitude from measured significant wave height and linear theory). *Nielsen*'s [1992] values for the transition to sheet flow, $\Psi = 156$ and $\theta \cong 1.0$, are based on wave-orbital velocity amplitude of regular waves. *Soulsby* [1997] noted (and it is observed here, Figure 7) that Nielsen's values are not compatible with each other. *Soulsby* [1997] gives $\theta_s \cong 0.8$ (the skin-friction Shields parameter) as being the approximate criterion for the transition to sheet flow in both steady flows and oscillatory flows. Here, the observed threshold is $\Psi \cong 150$ and $\theta \cong 0.5$. Although lower than most values noted above, this is in agreement with the observations of *Li and Amos* [1999], who found that Nielsen's estimate of $\theta \cong 1.0$ was accurate for only the smallest grain sizes (D = 0.01 mm) and that the threshold for sheet flow decreased with increasing grain size. They developed an empirical expression for critical Shields' parameter in purely oscillatory flow as a function of grain size, based on many different observations found in the literature. From this, the predicted critical value for the conditions at Duck is $\theta \cong 0.8$. *Li and Amos* [1999] also found that the critical sheet flow Shields' parameter was about 50% smaller under combined waves and currents (a small subset of the observations that they compiled) than that predicted for pure waves, even after accounting for combined flow nonlinearities by calculating shear stress using work by *Grant and Madsen* [1986]. They presented an empirical expression using only the combined flow data that predicts a critical value of $\theta \cong 0.4$ for the observations presented here. *Li and Amos* [1999] could not provide an explanation for the latter effect.

[27] The spatial patterns and associated offshore wave heights suggest the intuitive hypothesis of a relationship between the flow field and the bed morphology. The gross observation that the bed becomes flat above a certain threshold supports that hypothesis. However, the observed weak relationship between mobility number, Shields' parameter, (or any other measure of the flow field) and RMS bed roughness is surprising. There are a number of possible factors affecting these observations. The fluid and bed observations are spatially separated by about 15 m, thus it is possible that the fluid measurements do not represent the local conditions over the bedforms. However, an examination was made of bed elevation changes below the current meters using collocated stationary sonar altimeters. This qualitative comparison indicates that there are similar types of bed features beneath the stationary altimeters and the CRAB-mounted altimeters about 85% of the time. Another explanation could be that sediment characteristics were not well resolved. Sediments were measured only twice during the experiment (collocated with the current meters), thus temporal and spatial variations in local sediment characteristics could be unresolved. The fluid characteristics were based on 3-hour averages, from the 3 hours preceding the bed measurement. It is assumed that the bed is in equilibrium with the flow, because almost all conditions are above the threshold of sediment motion (Figure 7) and therefore, sediment is always moving. However, under very low energy conditions or conditions that are changing quickly, an average from the previous 3 hours may not

represent the appropriate flow conditions for the observed bed configuration.

4. Conclusions

[28] Observations indicate that large bedforms occur frequently in the nearshore and that their distribution is highly variable. These features have been observed in Oregon, the Great Lakes and North Carolina [*Clifton et al.*, 1971; *Hay and Wilson*, 1994; *Thornton et al.*, 1998] suggesting that the bedform processes are similar in surf zones with very different characteristics (e.g., slope, grain size, wave energy, etc.). In general, spectra of bedforms in the nearshore have a broad peak at low wave number (corresponding wavelength 1–5 m) and decay at high wave numbers, meaning that large bedforms, when present, dominate the energy spectrum (for wavelengths <10 m) and that their length scales are variable. Bedforms are largest and most prevalent inside the surf zone (water depths <2 m) and their amplitudes and occurrence decrease offshore. However, the variability (both spatial and temporal) of the bedforms is also largest in shallow water.

[29] The RMS bed roughness shows a weak dependence on mobility number and Shields parameter. For $30 < \Psi < 150$ both small ripples and large ripples can exist, but no sharp transition is observed between a small ripple regime and a large ripple regime. Large bedforms (RMS amplitude >2 cm) disappear for $\Psi > 150$ and $\theta > 0.5$. These observed values are slightly lower than those found in much of the literature [e.g., *Nielsen*, 1992; *Soulsby*, 1997]. However, it is in agreement with the work of *Li and Amos* [1999] who compiled data from many studies and found critical Shields' parameter to depend on grain size and to be lower in combined flows than that for waves alone.

[30] **Acknowledgments.** This research was supported by the Office of Naval Research (Coastal Dynamics and Mine Burial Programs), the National Science Foundation (Marine Geology and Geophysics), and the National Research Council. The array was designed, fabricated, deployed, and maintained by Rob Wyland, Jim Stockel and Ron Cowen. The current meter data was generously provided by Steve Elgar (WHOI). The staff at the US Army Corps of Engineers Field Research Facility provided excellent logistical support with the CRAB.

References

Allen, J. R. L., *Current Ripples: Their Relation to Patterns of Water and Sediment Motion*, 433 pp., North-Holland, New York, 1968.

Bailard, J., An energetics total load sediment transport model for a plane sloping beach, *J. Geophys. Res.*, *86*, 10,938–10,954, 1981.

Clifton, H. E., Wave-formed sedimentary structures—A conceptual model, in *Beach and Nearshore Sedimentation*, edited by R. A. Davis Jr. and R. L. Ethington, *SEPM Spec. Publ. 24*, pp. 126–148, 1976.

Clifton, H. E., R. E. Hunter, and R. L. Phillips, Depositional structures and processes in the non-barred high-energy nearshore, *J. Sediment. Petrol.*, *41*(3), 651–670, 1971.

Davidson-Arnott, R. G. D., and B. Greenwood, Facies relationships on a barred coast, Kouchibouquac Bay, New Brunswick, Canada, in *Beach and Nearshore Sedimentation*, edited by R. A. Davis Jr. and R. L. Ethington, *SEPM Spec. Publ. 24*, pp. 149–169, 1976.

Dingler, J. R., and D. L. Inman, Wave formed ripples in nearshore sands, paper presented at 15th Coastal Engineering Conference, Am. Soc. Civ. Eng., New York, 1976.

Elgar, S., R. T. Guza, and M. Freilich, Eulerian measurements of horizontal accelerations in shoaling gravity waves, *J. Geophys. Res.*, *93*, 9261–9269, 1988.

Fredsoe, J., Turbulent boundary layer in wave-current motion, *J. Hydraul. Eng.*, *110*, 1103–1120, 1984.

Fredsoe, J., and R. Deigaard, *Mechanics of Coastal Sediment Transport*, *Adv. Ser. Ocean Eng.*, vol. 3, 369 pp., World Sci., River Edge, N. J., 1992.

Gallagher, E. L., W. Boyd, S. Elgar, R. T. Guza, and B. Woodward, Performance of a sonar altimeter in the nearshore, *Mar. Geol.*, *133*, 241–248, 1996.

Grant, W. D., and O. S. Madsen, Combined wave and current interaction with a rough bottom, *J. Geophys. Res.*, *84*, 1797–1808, 1979.

Grant, W. D., and O. S. Madsen, The continental shelf bottom boundary layer, *Ann. Rev. Fluid Mech.*, *18*, 265–305, 1986.

Greenwood, B., and D. J. Sherman, Hummocky cross-stratification in the surf zone: Flow parameters and bedding genesis, *Sedimentology*, *33*, 33–45, 1986.

Hay, A. E., and D. J. Wilson, Rotary side scan images of nearshore bedform evolution during a storm, *Mar. Geol.*, *119*, 57–65, 1994.

Li, M. Z., and C. L. Amos, Sheet flow and large wave ripples under combined waves and currents: Field observations, model prediction and effects on boundary layer dynamics, *Cont. Shelf Res.*, *19*, 637–663, 1999.

Middleton, G. V., and J. B. Southard, *Mechanics of Sediment Transport*, *SEPM Short Course*, *3*, 1984.

Nicholson, J., I. Broker, J. A. Roelvink, D. Price, J. M. Tanguy, and L. Moreno, Intercomparison of coastal area morphodynamic models, *Coastal Eng.*, *31*, 97–123, 1997.

Nielsen, P., Dynamics and geometry of wave-generated ripples, *J. Geophys. Res.*, *86*, 6467–6472, 1981.

Nielsen, P., *Coastal Bottom Boundary Layers and Sediment Transport*, *Adv. Ser. Ocean Eng.*, vol. 4, 324 pp, World Sci., River Edge, N. J., 1992.

Raudkivi, A. J., *Loose Boundary Hydraulics*, 538 pp., Pergamon, New York, 1990.

Reineck, H. E., and I. B. Singh, *Depositional Sedimentary Environments*, 439 pp., Springer-Verlag, New York, 1975.

Soulsby, R. L., *Dynamics of Marine Sands*, Thomas Telford, London, 1997.

Soulsby, R. L., L. Hamm, G. Klopman, D. Myrhaug, R. R. Simons, and G. P. Thomas, Wave-current interactions within and outside the bottom boundary layer, *Coastal Eng.*, *21*, 41–69, 1993.

Southard, J. B., J. M. Lambie, D. C. Federico, H. T. Pile, and C. R. Weidman, Experiments on bed configurations in fine sands under bidirectional purely oscillatory flow and the origin of hummocky cross-stratification, *J. Sediment. Petrol.*, *60*, 1–17, 1990.

Thornton, E. B., J. L. Swayne, and J. R. Dingler, Small-scale morphology related to waves and currents across the surf zone, *Mar. Geol.*, *145*, 173–196, 1998.

Young, I. R., and R. M. Gorman, Measurement of the evolution of ocean wave spectra due to bottom friction, *J. Geophys. Res.*, *100*, 10,987–11,004, 1995.

E. Gallagher, Department of Biology, Franklin and Marshall College, PO Box 3003, Lancaster, PA 17604, USA. (edith.gallagher@fandm.edu)

T. P. Stanton and E. B. Thornton, Oceanography Department, Code OC, Naval Postgraduate School, 833 Dyer Road, Room 328, Monterey, CA 93943-5122, USA. (stanton@oc.nps.navy.mil; thornton@oc.nps.navy.mil)